ACS OMEGA

http://pubs.acs.org/journal/acsodf

Article

Corrosion Behavior of 1D and 2D Polymorphs of Boron Nitride Ceramic

Tony Thomas and Arvind Agarwal*

Cite This: *ACS Omega* 2023, 8, 3184−3189

Read Online

ACCESS | Metrics & More | Article Recommendations

ABSTRACT: This study reports a fundamental electrochemical study to understand the corrosion behavior of 1D bulk, free-standing 1D boron nanotube (BNNT) buckypaper and compare it with a sintered 2D hBN nanoplatelet (BNNP) pellet. Tafel analysis indicates that 1D BNNT has superior corrosion resistance with a lower corrosion rate of 0.0026 mils per year (mpy). 2D BNNP, although having similar chemistry to 1D BNNT, resulted in an increased (40 times) corrosion rate of 0.107 mpy. The higher surface area and aspect ratio of BNNT drastically influenced the corrosion kinetics. The scientific outcomes will enable the better design of novel hBN-based corrosion-resistant materials.

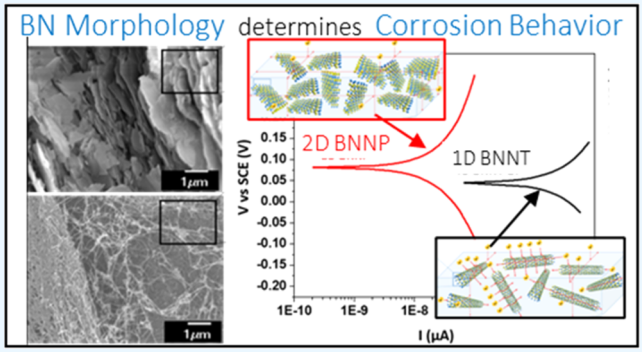

1. INTRODUCTION

Hexagonal boron nitride (hBN) is an electrically insulating isomorph of graphite, where the boron and nitrogen atoms form the A and B sub-lattices. Like graphite, hBN possesses high thermal conductivity,[1,2] mechanical strength, ultra-high impermeable properties,[3] and oxidation resistance.[4] The position of B and N atoms results in a reduced electro-delocalization in their bond energies, resulting in a wide bandgap of 5.96 eV, making hBN electrically insulating.[5] Due to their highly electrically insulating nature, hBN does not promote galvanic corrosion of the underlying materials. Hence, recent research has focused on applying hBN as a protective barrier material against the corrosion of metals and oxidation under extreme conditions.[6−10]

Initial studies report corrosion-inhibiting properties of hBN when BN particles are directly coated on metal substrates or as additives with polymers.[11−18] However, a few studies concluded that thick nanolaminate BN particles increase the corrosion rate of composite materials.[11] Liu et al. confirmed that the ultrathin-grown BN's effectiveness on Ni acted as an effective oxidation-resistant coating in an aggressive atmosphere up to 1100 °C.[18] Unlike the thick BN particles, the ultrathin BN coating offered a more interface between BN and Ni, reducing the electrochemical reaction rate. This study brought a new approach to corrosion mechanisms regarding the surface morphology and surface area of the barrier material. Subsequently, 2D boron nitride nanosheets (BNNS) have been explored for anticorrosion applications.[19−21] Compared to traditional micron-sized irregular BN particles, 2D BNNS's large lateral dimension offers greater interfacing with the host material, increasing the corrosion resistance in such systems. Yi et al.,[22] in their study on size-selected BNNS coating on a polymer, concluded that larger BNNS (~21.4 μm^2) greatly enhanced the corrosion resistance of the polymer. Hexagonal BN's proactive anticorrosive property is directly correlated with its surface morphology and area.[11−22]

Bulk, free-standing 1D boron nanotubes (BNNTs) fabricated as 100% BNNT and oriented randomly in-plane are commercially available as BNNT buckypaper (BP).[23−26] They are analogous to carbon nanotubes but offer multifunctional advantages, including piezoelectricity, electrical insulation, high-temperature stability, and neutron absorption.[27,28] Compared to 2D hBN nanoplatelet (BNNP), 1D BNNT is arranged randomly into a porous 3D structure and offers a substantially greater surface area. Previous research studies[11−22] concluded that hBN with a high surface area offers increased corrosion resistance due to higher interfacing with the underlying material. Yet, BNNTs are not recognized as corrosion-inhibiting additives. This is due to a lack of fundamental knowledge of the electrochemical behavior of free-standing hBN polymorphs. Thus, the present study focuses on if BNNTs display improved corrosion resistance. A fundamental electrochemical study is reported to understand the corrosion behavior of free-standing BNNT-BP and

Received: October 14, 2022
Accepted: December 30, 2022
Published: January 9, 2023

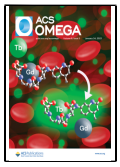

compare it with 2D hBN via the DC potentiodynamic corrosion test. The study reveals how the surface morphology and surface area of hBN polymorphs influence the electrochemical reaction in corrosion inhibition. A quantitative analysis of Tafel parameters is carried out to establish the effect of polymorphism on the electrochemical stability of hBN in a mild simulated seawater environment.

2. RESULTS AND DISCUSSION

The corrosion behavior of 1D BNNT-BP and 2D BNNP was studied in a 0.1 normal sodium chloride (3.5 wt % NaCl or simulated seawater) solution environment at room temperature and pressure. The samples were conditioned in the electrolyte for 60 min to reach a stable open-circuit potential (OCP). Figure 1a shows the OCP of BNNT-BP and BNNP.

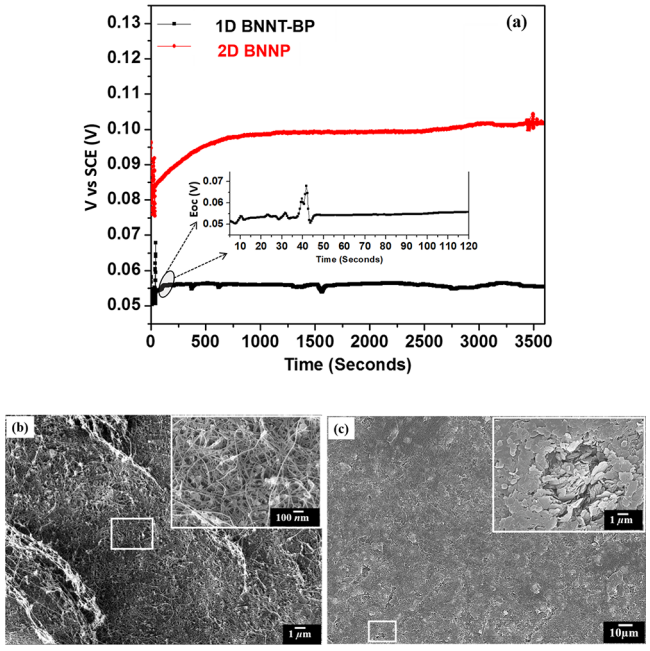

Figure 1. OCPs of 1D BNNT-BP and 2D BNNP. Inset showing the OCP voltage for 1D BNNT-BP up to 120 s. SEM images of (b) as-received 1D BNNT-BP. Inset showing the magnified BNNT morphology within the highlighted white rectangle. The nodules are residual boron nanoparticles formed during the BNNT synthesis and (c) as-synthesized dense 2D BNNP pellet surface. Inset showing the porosities on the dense 2D BNNP pellet and the 2D structure of BNNP.

The OCP, the corrosion potential (Ecorr), indicates the electromotive force or voltage conducted by the materials' active surface. BNNT-BP has an active surface area of 1340 cm^2 and an E_{corr} of 55.46 mV, while BNNP, with a lower active surface area of 0.75 cm^2, recorded a higher E_{corr} of 101.7 mV. Although BNNT-BP and BNNP test samples have 3D structures, their basic microstructure is 1D and 2D, respectively, as shown in Figure 1b,c. The nanotubes composing BNNT-BP have a higher aspect ratio, with the length of the nanotubes varying between 1 and 100 μm with an average diameter of 5 nm, as shown in Figure 1b. Hence, the resultant BNNT-BP has a high surface area and offers more resistance to the flow of charges, unlike low surface area BNNP. It is also observed from Figure 1a inset that BNNT-BP reaches a stable OCP of ∼55 mV in ∼1 min, whereas 2D BNNP starts at an OCP of 60 mV and gradually stabilizes after 20 min at about 101.7 mV. The variation in the OCP stabilization time can be attributed to the porosity present and the particle morphology in both the test materials, which affect the electrolyte absorption. A stable OCP is achieved when the interaction between the test sample and the environment is at equilibrium. BNNT-BP is highly porous due to their randomly oriented nanotube structure, and BNNP consolidated by SPS had 10% porosity,[29] as shown in Figure 1b,c, respectively. The hollow tubes of the BNNT-BP aggravate the electrolyte absorption by the capillary effect, thus quickly equilibrating with the environment. On the other hand, BNNP is only 10% porous, with randomly shaped pores exposing the nanolaminate layers to the electrolyte (refer to the inset in Figure 1c). The absorption of electrolytes into nanolaminate BNNP is slow compared to the capillary effect induced by BNNT, thus increasing the time for OCP stabilization in 2D BNNP.

After the samples recorded a stable OCP, a potentiodynamic test was carried out to analyze the effect of hBN polymorphs on corrosion kinetics. Figure 2a shows a comparative Tafel plot of BNNT-BP and BNNP. Tafel analysis was performed as shown in Figure 2b,c to extract the Tafel data for BNNT-BP and BNNP. From Figure 2a, it can be observed that the I_{corr} values of BNNT-BP and BNNP are 4.13 ± 0.1 μA and 0.114 ± 0.044 μA, respectively. BNNT-BP exhibits high anodic and cathodic currents than BNNP. The current density of BNNT-BP and BNNP is 0.0031 and 0.152 $\mu A/cm^2$. Due to the high surface area, BNNT-BP exhibits low current density. The E_{corr} values of BNNT-BP and BNNP are 45.9 ± 0.1 mV and 84.43 ± 19.35 mV, respectively. The lower E_{corr}, along with the lower current density of BNNT-BP, indicates excellent antioxidation behavior of BNNT-BP compared to BNNP. These subtle electrochemical variations between BNNT-BP and BNNP translate to better corrosion properties. The corrosion rate of BNNT-BP (0.0026 mpy) is ∼40 times lower than that of BNNP (0.107 mpy). Although the material has similar chemistry, the morphology of BN dramatically influences the active surface area of the materials. For uniform corrosion, the corrosion rate (CR) is dictated by the following relation

$$CR = \frac{I_{corr} K EW}{\rho A} \quad (1)$$

where K = 3272 mm/A·cm·year, EW is the equivalent weight of hBN (8.27 g/equiv), ρ is the density of hBN (2.1 g/cm^3), and A is the active surface area. From eq 1, it can be inferred that CR is indirectly proportional to the surface area of the material and directly proportional to the I_{corr} of the material. Hence, the high surface area BNNT-BP (∼1340 cm^2) lowers the corrosion kinetics compared to the low surface area BNNP (∼0.75 cm^2).

Figure 3 is the schematic explaining how high surface area BNNTs drastically reduce the CR compared to low surface area BNNPs. Corroding metals form metal ions and release a free electron in a metal corrosion process. These free electrons reduce the oxygen in the environment to oxygen ions (O^{2-}). The metal ions can react with O^{2-} to form respective oxides. However, if there is a layer of an insulating material such as hBN, an inherently electrically insulating material traps the free electrons at the interface between the metal and the protective layer, thus preventing an oxidation reaction.[30] High surface area BNNT can trap more electrons and prevent oxidation and reduction reactions with the environment more effectively than low surface area BNNP as represented by Figure 3. Also, in the case of BNNT, the electromotive force or the ability to

https://doi.org/10.1021/acsomega.2c06477
ACS Omega 2023, 8, 3184−3189

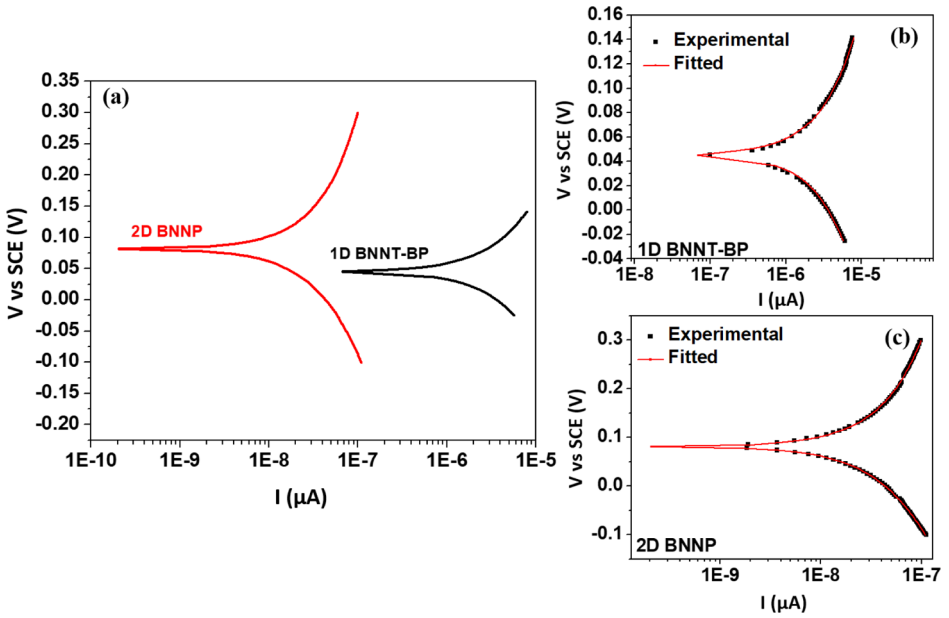

Figure 2. Tafel plots of 1D BNNT-BP and 2D BNNP were obtained from the potentiodynamic test. (a) Comparative Tafel plots, (b) experimental and fitted data plots of 1D BNNT-BP, and (c) experimental and fitted data plots of 2D BNNP.

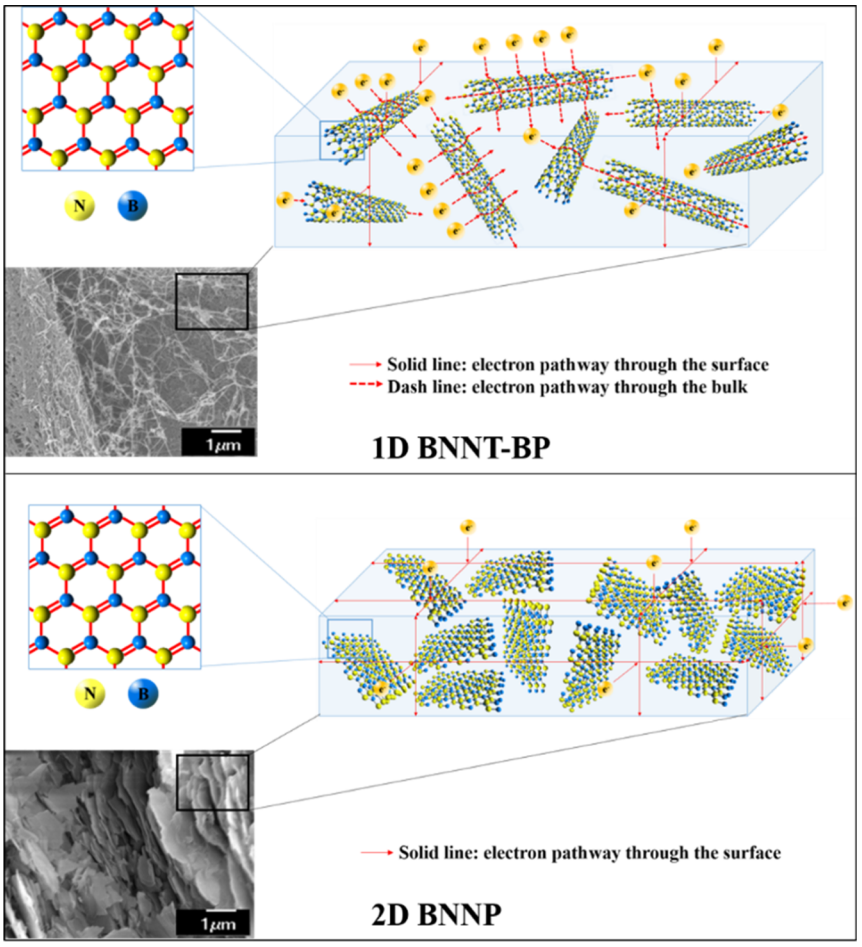

Figure 3. Schematic showing charge-transfer effects in (a) BNNT and (b) BNNP.

conduct charges is comparatively lower than that of BNNP, as found by OCP analysis (refer to Figure 1a). Both materials offer low CR, but BNNT provides more corrosion protection than BNNP due to more charge-hindering surfaces.

Figure 4a,b shows the XRD diffractogram for BNNT-BP before and after the corrosion. The similarity in the XRD diffraction emphasizes the absence of oxidation or reduction reaction in BNNT-BP. However, for 2D BNNP, the intensity

https://doi.org/10.1021/acsomega.2c06477
ACS Omega 2023, 8, 3184−3189

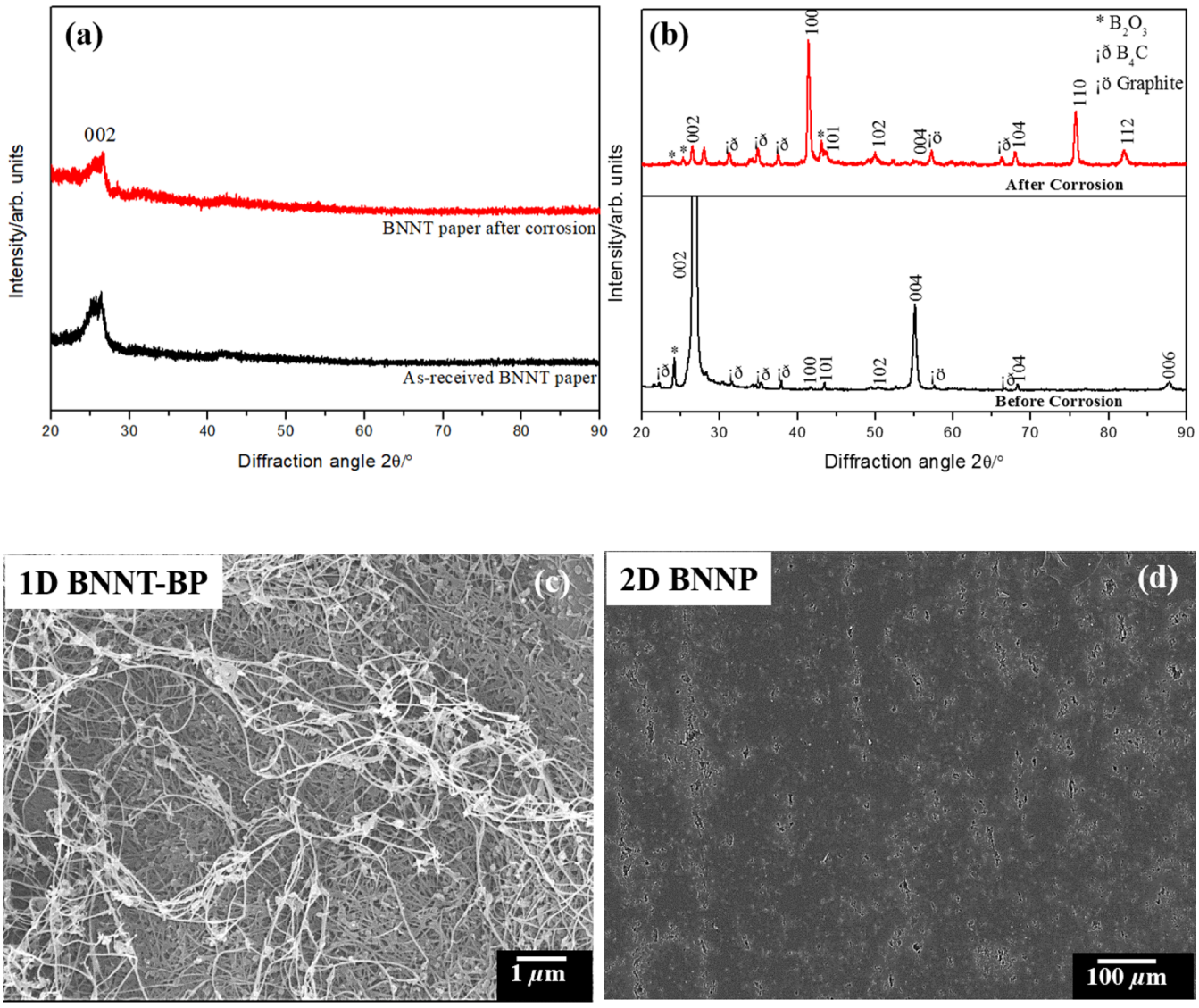

Figure 4. X-ray diffraction patterns for (a) 1D-BNNT BP and (b) sintered 2D-BNNP pellets before and after corrosion. Post-corrosion SEM images of (c) 1D-BNNT BP and (d) sintered 2D-BNNP.

of the (002) and (004) planes reduces, while that of the (100) plane increases after corrosion. Although there was no noticeable weight change in 2D BNNP after corrosion, the variation in the peak intensities can give a clue of inter-planar material reduction, suggesting active corrosion in 2D BNNP. Secondary peaks of B_2O_2 and B_4C can be seen in a 2D BNNP before and after corrosion diffractogram. Oxygen and carbon impurities are often present in the BN crystal structure.[31]

SEM imaging was performed to observe and analyze the formation of pits or oxide layers on the samples after corrosion. Figure 4c,d shows the micrographs of BNNT-BP and BNNP, respectively, after the potentiodynamic corrosion tests. After corrosion, no noticeable pits or unusual morphology were detected on the BNNT-BP and BNNP samples (refer to Figure 1b,c for SEM images before the corrosion test). Both samples exhibit excellent corrosion-resisting properties. Still, BNNT-BP has precedence over BNNP due to its high surface area, offering more electrically resistive channels than BNNP. As CR is a function of I_{corr} and surface area, a highly resistive material with a high surface area like 1D BNNT-BP can protect metals and polymers against corrosion.

3. CONCLUSIONS

A fundamental electrochemical study is conducted to understand and analyze the corrosion behavior of 1D BNNT-BP and 2D BNNP via the DC potentiodynamic corrosion test. BNNT-BP has a higher active surface area, offering more electrically resistive channels than BNNP. The high surface area of BNNT-BP drastically influenced the corrosion kinetics of the hBN system, which resulted in ∼40 times lower CR than BNNP. The study conducted establishes a fundamental understanding of how the polymorphs of hBN, that is, 1D BNNT-BP and 2D BNNP, influence the corrosion kinetics to inhibit the corrosion reaction.

4. EXPERIMENTAL SECTION

1D BNNT-BP was purchased from TEKNA, Quebec, Canada. Commercial BNNT-BP is highly porous, with a surface area of >100 m^2/g and a thickness of 75 μm. The length of the nanotubes varied between 1 and 100 μm and had an average diameter of 5 nm. The 2D boron nitride nanoplatelet (BNNP) powder was purchased from pH Matter LLC, OH, USA. The 2D BNNP powder had a surface area of >50 m^2/g. For the

https://doi.org/10.1021/acsomega.2c06477
ACS Omega 2023, 8, 3184−3189

corrosion test, the 2D BNNP powder was consolidated into 20 mm-wide and 2 mm-thick cylindrical pellets by Spark Plasma Sintering. The processing parameters are reported elsewhere.[29] The test samples were cut into a ~6.5 × 3.5 mm^2 rectangular specimen. Porous BNNT-BP had a thickness of 75 μm and offered an active surface area of ~1340 cm^2. The dense 2D BNNP pellet had a thickness of 2 mm and offered an active surface area of ~0.75 cm^2.

A three-electrode configuration, immersion type, and DC potentiodynamic (ASTM G5) corrosion test was performed in a 0.1 normal sodium chloride (3.5 wt % NaCl or simulated seawater) solution (Aqua Solutions, TX, USA) in a Eurocell corrosion cell (Gamry Instruments, PA, USA). Saturated calomel electrode in potassium chloride (KCl) solution was used as a reference electrode, and a carbon rod was used as a counter electrode. Gamry Potentiostat Interface 1000 and Gamry Framework were used to run the DC potentiodynamic tests. The BNNT-BP sample is fragile owing to a low thickness of approximately 75 μm. Hence, the usual sample securing system, typically by screw, can damage the sample and result in a non-uniform surface contact with the sample holder. Colloidal silver paste (PELCO, Product no. 16032, Ted Pella, INC, USA) was used to stick the BNNT-BP sample onto the Eurocell sample holder and ensure maximum surface contact. The silver paste was air-dried before the electrochemical testing. The dense 2D BNNP pellet sample was secured to the Eurocell sample holder by the in-built screw system. No additional sample preparation was performed on the 2D BNNP test sample. For BNNT-BP, a voltage sweep was performed from −0.25 to 0.15 V at a scan rate of 1 mV/s. For 2D BNNP, a voltage sweep from −0.25 to 0.3 V at a scan rate of 1 mV/s was employed. Since BNNT-BP and 2D BNNP exhibited different OCPs, the test potential difference had to be set differently to minimize the extensive cathodic reaction. Tafel analysis was performed using the Gamry Echem Analyst. At least three samples of each hBN polymorph were tested, and their average results were reported. An X-ray diffractometer (Siemen D500) was employed to analyze the phases before and after corrosion. The morphology of the samples, before and after corrosion, was analyzed using the JEOL JSM-6330F field emission scanning electron microscope.

AUTHOR INFORMATION

Corresponding Author

Arvind Agarwal − *Plasma Forming Laboratory, Mechanical and Materials Engineering, Florida International University, Miami, Florida 33174, United States;* orcid.org/0000-0002-7052-653X; Email: agarwala@fiu.edu

Author

Tony Thomas − *Plasma Forming Laboratory, Mechanical and Materials Engineering, Florida International University, Miami, Florida 33174, United States*

Complete contact information is available at: https://pubs.acs.org/10.1021/acsomega.2c06477

Notes

The authors declare no competing financial interest.

ACKNOWLEDGMENTS

The usage of facilities at the Advanced Materials Engineering Research Institute (AMERI) is recognized for the research reported in this study. The authors acknowledge the Office of Naval Research grant # N00014-17-1-2563.

REFERENCES

(1) Shen, H.; Guo, J.; Wang, H.; Zhao, N.; Xu, J. Bioinspired modification of h-BN for high thermal conductive composite films with aligned structure. *ACS Appl. Mater. Interfaces* **2015**, *7*, 5701−5708.

(2) Yu, J.; Huang, X.; Wu, C.; Wu, X.; Wang, G.; Jiang, P. Interfacial modification of boron nitride nanoplatelets for epoxy composites with improved thermal properties. *Polymer* **2012**, *53*, 471−480.

(3) Husain, E.; Narayanan, T. N.; Taha-Tijerina, J. J.; Vinod, S.; Vajtai, R.; Ajayan, P. M. Marine corrosion protective coatings of hexagonal boron nitride thin films on stainless steel. *ACS Appl. Mater. Interfaces* **2013**, *5*, 4129−4135.

(4) Yi, M.; Shen, Z.; Zhao, X.; Liang, S.; Liu, L. Boron nitride nanosheets as oxygen-atom corrosion protective coatings. *Appl. Phys. Lett.* **2014**, *104*, 143101.

(5) Watanabe, K.; Taniguchi, T.; Kanda, H. Direct-bandgap properties and evidence for ultraviolet lasing of hexagonal boron nitride single crystal. *Nat. Mater.* **2004**, *3*, 404−409.

(6) Zhao, H.; Ding, J.; Yu, H. Advanced Bio-Based UV-Curable Anticorrosive Coatings Reinforced by hBN. *ChemistrySelect* **2018**, *3*, 11277−11283.

(7) Chilkoor, G.; Jawaharraj, K.; Vemuri, B.; Kutana, A.; Tripathi, M.; Kota, D.; Arif, T.; Filleter, T.; Dalton, A. B.; Yakobson, B. I.; Meyyappan, M.; Rahman, M. M.; Ajayan, P. M.; Gadhamshetty, V. Hexagonal boron nitride for sulfur corrosion inhibition. *ACS Nano* **2020**, *14*, 14809−14819.

(8) Mahvash, F.; Eissa, S.; Bordjiba, T.; Tavares, A. C.; Szkopek, T.; Siaj, M. Corrosion resistance of monolayer hexagonal boron nitride on copper. *Sci. Rep.* **2017**, *7*, 42139.

(9) Dadvand, M.; Savadogo, O. Effect of hBN on Corrosion and Wear Performances of DC Electrodeposited NiW and NiW−SiC on Brass Substrates. *Coatings* **2022**, *12*, 1011.

(10) Galbiati, M.; Stoot, A. C.; Mackenzie, D. M. A.; Bøggild, P.; Camilli, L. Real-time oxide evolution of copper protected by graphene and boron nitride barriers. *Sci. Rep.* **2017**, *7*, 39770.

(11) Dikici, B.; Ozdemir, I. FeB and FeB/h-BN based anti-corrosive composite coatings for aluminum alloys. *Anti-Corros. Methods Mater.* **2012**, *59*, 246−254.

(12) Husain, E.; Narayanan, T. N.; Taha-Tijerina, J. J.; Vinod, S.; Vajtai, R.; Ajayan, P. M. Marine corrosion protective coatings of hexagonal boron nitride thin films on stainless. *ACS Appl. Mater. Interfaces* **2013**, *5*, 4129−4135.

(13) Gyawali, G.; Adhikari, R.; Kim, H. S.; Cho, H. B.; Lee, S. W. Effect of h-BN nanosheets co-deposition on electrochemical corrosion behavior of electrodeposited nickel composite coatings. *ECS Electrochem. Lett.* **2012**, *2*, C7.

(14) Kumar, C. P.; Venkatesha, T. V. Characterization and corrosion behavior of Electrodeposited Zn and Zn-BN coatings. *Synth. React. Inorg., Met.-Org., Nano-Met. Chem.* **2012**, *42*, 351−359.

(15) Li, G.; Chen, L.; An, Y.; Gao, M.; Zhou, H.; Chen, J. Investigating the effect of polytetrafluoroethylene on the tribological properties and corrosion resistance of epoxy/hydroxylated hexagonal boron nitride composite coatings. *Corros. Sci.* **2023**, *210*, 110820.

(16) Joseph, A.; Gautham, V.; Akshay, K. S.; Sajith, V. 2D MoS2-hBN hybrid coatings for enhanced corrosion resistance of solid lubricant coatings. *Surf. Coat. Technol.* **2022**, *443*, 128612.

(17) Tang, G.; Hou, X.; Wang, Y.; Yan, Z.; Ren, T.; Ma, L.; Huang, C.; Wang, C. Hexagonal Boron Nitride/Polyaniline Nanocomposites for Anticorrosive Waterborne Epoxy Coatings. *ACS Appl. Nano Mater.* **2021**, *5*, 361−372.

(18) Liu, Z.; Gong, Y.; Zhou, W.; Ma, L.; Yu, J.; Idrobo, J. C.; Jung, P. M.; MacDonald, A. H.; Vajtai, R.; Lou, J.; Ajayan, P. M. Ultrathin high-temperature oxidation-resistant coatings of hexagonal boron nitride. *Nat. Commun.* **2013**, *4*, 2541−2548.

(19) Liu, L.; Shen, Z.; Zheng, Y.; Yi, M.; Zhang, X.; Ma, S. Boron nitride nanosheets with controlled size and thickness for enhancing

mechanical properties and atomic oxygen erosion resistance. *RSC Adv.* **2014**, *4*, 37726−37732.
(20) Yi, M.; Shen, Z.; Zhao, X.; Liang, S.; Liu, L. Boron nitride nanosheets as oxygen-atom corrosion protective coatings. *Appl. Phys. Lett.* **2014**, *104*, 143101.
(21) Yu, Y.; Cui, M.; Zheng, W.; Zhao, H. Eco-friendly functionalization of hexagonal boron nitride nanosheets with carbon dots towards the reinforcement of the protective performance of water-borne epoxy coatings. *New J. Chem.* **2022**, *46*, 6330−6342.
(22) Yi, M.; Shen, Z.; Liu, L.; Liang, S. Size-selected boron nitride nanosheets as oxygen-atom corrosion resistant fillers. *RSC Adv.* **2015**, *5*, 2983−2987.
(23) Nautiyal, P.; Gupta, A.; Seal, S.; Boesl, B.; Agarwal, A. Reactive wetting and filling of boron nitride nanotubes by molten aluminum during equilibrium solidification. *Acta Mater.* **2017**, *126*, 124−131.
(24) Nautiyal, P.; Loganathan, A.; Agrawal, R.; Boesl, B.; Wang, C.; Agarwal, A. Oxidative unzipping and transformation of high aspect ratio boron nitride nanotubes into "white graphene oxide" platelets. *Sci. Rep.* **2016**, *6*, 29498.
(25) Nautiyal, P.; Zhang, C.; Boesl, B.; Agarwal, A. Non-equilibrium wetting and capture of boron nitride nanotubes in molten aluminum during plasma spray. *Scr. Mater.* **2018**, *151*, 71−75.
(26) Antillon, M.; Nautiyal, P.; Loganathan, A.; Boesl, B.; Agarwal, A. Strengthening in boron nitride nanotube reinforced aluminum composites prepared by roll bonding. *Adv. Eng. Mater.* **2018**, *20*, 1800122.
(27) *Nanotube Super Fiber Materials: Changing Engineering Design*, 1st ed.; Schulz, M. J.; Shanov, V.; Yin, Z., Eds.; William Andrew: Oxford, U.K., 2014; pp 267−287.
(28) Meng, W.; Huang, Y.; Fu, Y.; Wang, Z.; Zhi, C. Polymer composites of boron nitride nanotubes and nanosheets. *J. Mater. Chem. C* **2014**, *2*, 10049−10061.
(29) Loganathan, A.; Sharma, A.; Rudolf, C.; Zhang, C.; Nautiyal, P.; Suwas, S.; Boesl, B.; Agarwal, A. In-situ deformation mechanism and orientation effects in sintered 2D boron nitride nanosheets. *Mater. Sci. Eng., A* **2017**, *708*, 440−450.
(30) Ge, X.; Sumboja, A.; Wuu, D.; An, T.; Li, B.; Goh, F. T.; Hor, Z.; Zong, Y.; Liu, Z. Oxygen reduction in alkaline media: from mechanisms to recent advances of catalysts. *ACS Catal.* **2015**, *5*, 4643−4667.
(31) Weston, L.; Wickramaratne, D.; Mackoit, M.; Alkauskas, A.; Van de Walle, C. G. Native point defects and impurities in hexagonal boron nitride. *Phys. Rev. B* **2018**, *97*, 214104.

https://doi.org/10.1021/acsomega.2c06477
ACS Omega 2023, 8, 3184−3189